Analysis and Experimental Testing of a New Type of Variable Stiffness Magnetic Spring with a Linear Stroke Length

Md Emrad Hossain
Department of Electrical and Computer Engineering Portland State University, Portland, OR, 97201, USA
mdemrad@pdx.edu

Jonathan Z. Bird
Department of Electrical and Computer Engineering Portland State University, Portland, OR, 97201, USA
jonathan.bird@ieee.org

Victor Albarran
Department of Electrical and Computer Engineering Portland State University, Portland, OR, 97201, USA
avictor@pdx.edu

Dawei Che
Department of Electrical and Computer Engineering Portland State University, Portland, OR, 97201, USA
dawei2@pdx.edu

2021 IEEE Energy Conversion Congress and Exposition (ECCE) | 978-1-7281-5135-9/21/$31.00 ©2021 IEEE | DOI: 10.1109/ECCE47101.2021.9595241

***Abstract* — In this paper a new type of variable stiffness magnetic spring is proposed. The magnetic spring is composed of radially magnetized outer rotor magnets coupled with axially magnetized inner cylindrical magnets. It is shown that this magnet arrangement creates a highly linear stroke length. By rotating the inner magnetic rotor, the stiffness of the spring can be adjusted. The force as a function of stroke length and torque required to adjust the stiffness were computed using finite element analysis and then verified using an experimental test setup.**

***Keywords*— elastic actuator, oscillating drivetrains, magnetic spring, negative stiffness, magnetic actuation, variable impedance, vibration isolation, variable stiffness.**

I. Introduction

New types of variable stiffness magnetic actuators are being investigated for use in robotic joints [1-5], exoskeleton devices [6], power generators [7, 8] and vibration isolators [9, 10]. It has been shown to be challenging to create a good range of stiffness adjustment using mechanical spring mechanisms [4, 11]. Often the mechanical based stiffness adjustment mechanisms are complex and bulky requiring, for instance, many mechanical springs [12] to create variable positive stiffness or a three-spring device to create a limited range of negative stiffness [13].

The non-contact operation of a variable stiffness magnetic actuator, also termed a magnetic spring, has the potential of overcoming many of the limitations encountered with their mechanical counterparts. Variable stiffness magnetic springs can be created by adjusting current excitation within a magnet device [7, 9, 10] however this results in the need to continually use power to maintain the stiffness change. A variable stiffness magnetic spring can also be created by using antagonistic north-south magnets [14], but using a direct magnet interface creates a highly non-linear stroke length [3, 14]. Recently a new type of variable stiffness magnetic spring was studied in [15] that exhibited a linear stroke length and had the ability for the stiffness to be adjusted via the rotation of the magnets [15]. To avoid power loss a mechanical brake can be used to thereby maintain a particular stiffness value indefinitely without power loss. It was shown in [15] that a relatively long linear stroke length could be created and unlike in other variable stiffness designs [16-18] the magnet actuator does not need to be combined with a mechanical spring in order to create a negative stiffness. This paper aims to build on the work presented in [15] by present a new magnet arrangement that increases the stroke length and improves the magnet design. An experimental test setup is used to validate the variable stiffness magnetic spring characteristics.

This research in funded in part by the Department of Energy's Office of Energy Efficiency and Renewable Energy (EERE) under the water power Technologies Office, Award number DE-EE0001837.

II. Dual Airgap Variable Stiffness Magnetic Spring

Based on the proof-of-principle work completed in [15] a dual-airgap variable stiffness magnetic spring was initially studied. Examples of a four pole-pair and one pole-pair variable stiffness magnetic spring version is shown in Fig. 1 and Fig. 2 respectively. The variable stiffness magnetic spring's linear stroke length is created via the center magnet reluctance force wanting to realign with the side magnets. The four pole-pair design achieves this by making the axial magnetized magnet length, h_z, the same length as the radial magnetized magnet length, h_r. Whilst the one pole-pair design makes the radial magnet length half the axial magnet length $h_z = 2h_r$. The peak stroke length, z_m, is determined by the height of the magnets. Due to the difference in magnet arrangement the zero-force position, for the four pole-pair design example, is at $z_t = h_z/2$. Whilst for the one pole pair design example the zero force is at $z_t = 0$. Example plots calculated using 3-D finite element analysis (FEA) for the force as a function of stroke length are shown in Fig. 3. Both the force profile at the peak positive and negative stiffness value is shown. The parameters shown in Table I were used. It was determined that a lower number of pole-pairs helps to increase the stroke length, but it is still difficult to achieve a linear stroke length greater than 30mm without having a very large force and very large magnets. The linearity of the

Authorized licensed use limited to: PORTLAND STATE UNIVERSITY LIBRARY. Downloaded on June 09,2024 at 03:02:12 UTC from IEEE Xplore. Restrictions apply.

stroke length is dependent on the radial thickness of the magnets, for the longer stroke lengths the magnet thickness must be increased.

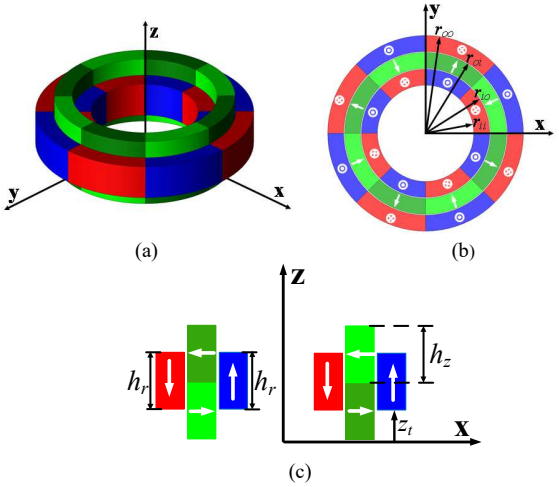

Fig. 1. (a) Perspective view, (b) plan view and (c) cut-through view of the 4-pole-pair dual-airgap coaxial VSMS.

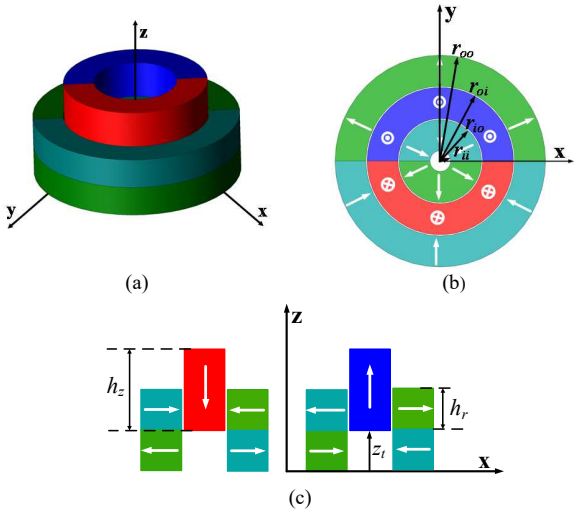

Fig. 2. (a) Perspective view, (b) plan axis view and (c) cut-through view of the one pole-pair dual-airgap VSMS

TABLE I
DUAL AIRGAP ADJUSTABLE STIFFNESS MAGNETIC SPRING PARAMETERS

Description		Value		Units
Pole pairs, p		4	1	-
Stroke length, z_m		10	30	mm
Inner rotor	Inner radius, r_{ii}	30	10	mm
	Outer radius r_{io}	40	40	mm
	Axial length, h_i	20	60	mm
Middle rotor	Axial length, h_m	40	60	mm
Outer rotor	Inner radius, r_{oi}	51	72	mm
	Outer radius r_{oo}	61	92	mm
	Magnet axial length, h_o	20	60	mm
Airgap		2	2	mm
Magnet grade (Nd-Fe-B)		N50		-

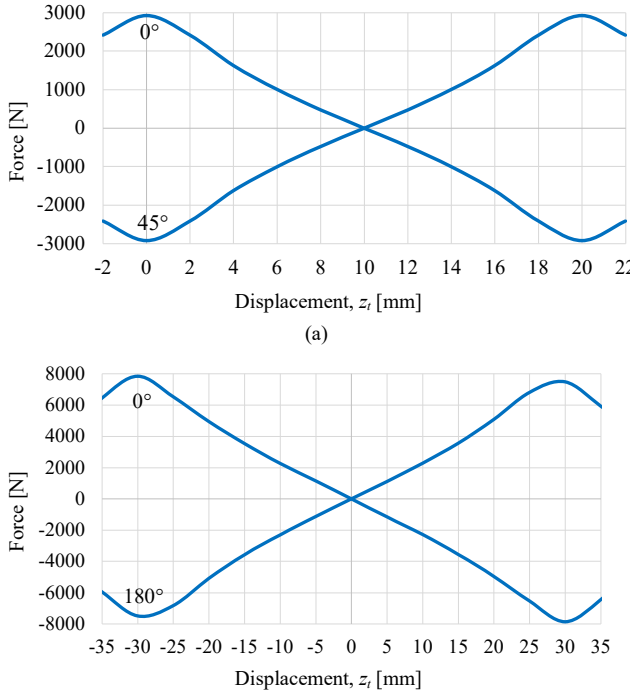

Fig. 3. Example 3-D finite element analysis results showing the maximum positive and negative stiffness force as a function of displacement for (a) the four and (b) the one pole-pair dual airgap coaxial VSMS.

III. SINGLE AIRGAP ADJUSTABLE STIFFNESS MAGNETIC SPRING

The dual-airgap magnetic spring design would be difficult to mechanically build due to the need to support the central moving magnets. Therefore, after much magnet arrangement analysis, a single-airgap, two pole-pair, variable stiffness magnetic spring was also invented, this design is shown in Fig. 4. The design is significantly easier to fabricate as the outer rotor magnets can be affixed to an outer ferromagnetic core and the inner rotor magnets can be supported by an inner non-magnetic core.

Utilizing a 3-D JMAG FEA model an energy density analysis was conducted on the single airgap design. To not make the force excessively high on the proof-of-principle design the outer rotor magnet radius and the stroke length were fixed at $(r_{oo}, z_m) = (70, 30)$ mm. As the magnet height is related to the stroke length the magnet heights are

$$h_r = 2h_z = z_m \tag{1}$$

The inner rotor magnet radii, (r_{ii}, r_{io}), were then swept. Since the airgap, $g = 0.5$mm, was not changed, and $r_{oi} = r_{io} + g$, there are then only two unknown inner rotor geometric values. The energy density sweep analysis at, 5mm step sizes, for the two inner rotor radii values is shown in Fig. 5. The energy density was computed by using:

$$E_d = \frac{k_m z_m^2}{2} \cdot \frac{1}{\rho_d \pi [2h_r(r_{oo}^2 - r_{oi}^2) + h_z(r_{io}^2 - r_{ii}^2)]} \tag{2}$$

Authorized licensed use limited to: PORTLAND STATE UNIVERSITY LIBRARY. Downloaded on June 09,2024 at 03:02:12 UTC from IEEE Xplore. Restrictions apply.

where k_m = maximum stiffness value and ρ_d = 7500 kg/m^3 is the magnet density. The peak energy density of E_d = 9.16 J/kg occurred at (r_{ii}, r_{io}) = (40,60). The coefficient of determination [19], defined as r^2, can be used to evaluate the level of linearity of the force. If r^2 =1 a line is completely linear, for the peak energy density design the linearity was computed to be r^2 = 0.9837. To improve the linearity of the stroke length the radius values (r_{ii}, r_{io}) = (30,56) were selected for the proof-of-principle prototype, using these radius values the linearity was improved r^2 = 0.9906 but the peak energy density decreased to E_d = 8.9 J/kg, a 2.83 % decrease. A summary of the peak energy density design and proof-of principle design geometric parameters are shown in Table II. A plot of the force and torque as a function of stroke length and rotary angle for the proof-of-principle design is shown in Fig. 6 and Fig.7 respectively. The stiffness can be adjusted between ± 146.2 N/mm. The force can be modelled by

$$F(z_t,\theta) = -k_m[\cos(p\theta)]\cdot z_t \qquad (3)$$

where p = 2 pole-pairs and k_m = peak stiffness value.

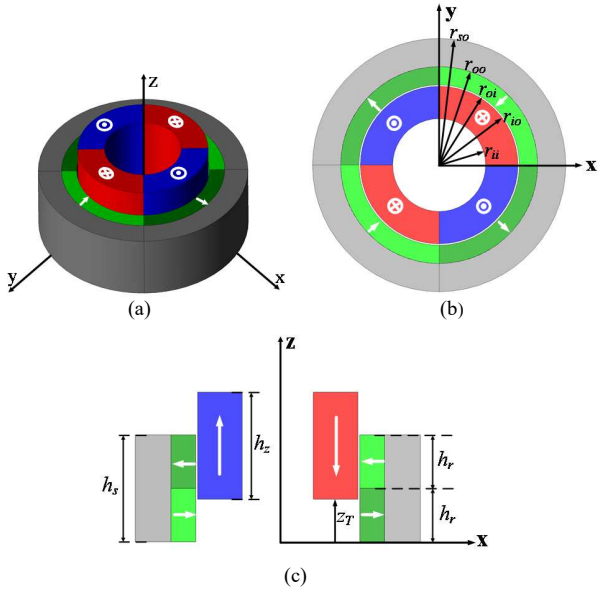

Fig. 4. (a) Perspective view, (b) plan view and (c) cut-through view of the newly invented single airgap variable stiffness magnetic spring. The outer (grey cylinder) is ferromagnetic providing a return flux path.

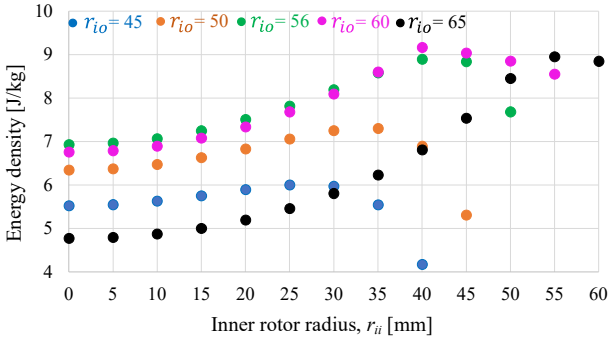

Fig. 5. Finite element analysis computed energy density as a function of inner rotor radius dimensions (r_{ii},r_{io}) when (r_{oo}, z_m) = (70,30).

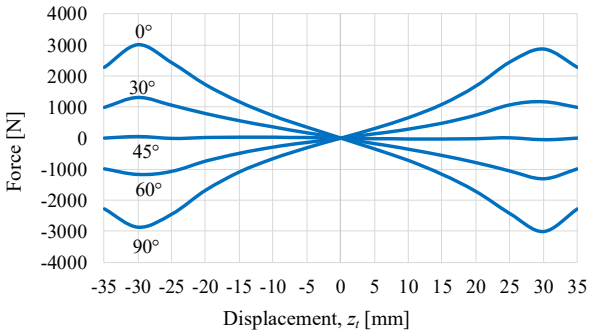

Fig. 6. Force as a function of displacement for the 30mm stroke length.

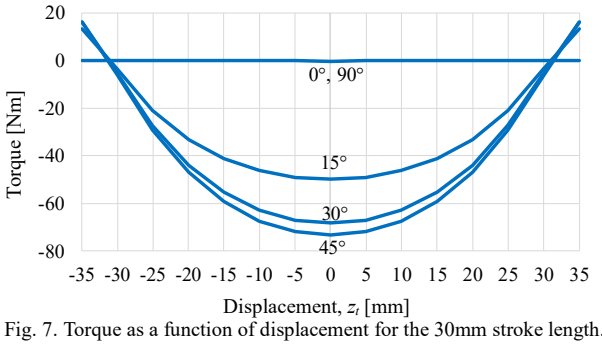

Fig. 7. Torque as a function of displacement for the 30mm stroke length.

TABLE II
SINGLE AIRGAP TWO POLE-PAIR ADJUSTABLE STIFFNESS MAGNETIC SPRING PARAMETERS

Description		**Peak Energy Density [mm]**	**Proof of Principle Design [mm]**
Stroke length, z_m		30	30
Inner rotor	Inner radius, r_{ii}	40	30
	Outer radius r_{io}	60	56
	Axial length, h_i	60	60
Outer rotor	Inner radius, r_{oi}	61	57
	Outer radius r_{oo}	70	70
	Magnet axial length, h_o	30	30
	Outer radius r_{so}	90	90
	Axial length, h_s	60	60
Airgap		1	1

IV. EXPERIMENTAL PROTOTYPE

The assembly drawing of the experimental proof-of-principle prototype is shown in Fig. 8 and the fully assembled variable stiffness magnetic spring is shown in Fig. 9(a). In the experimental design it was decided to make the outer magnet assembly translate and the inner rotor rotate. The complete experimental test stand is shown in Fig. 9(b). The torque required to adjust the stiffness was measured by utilizing a Futek (model TRS605) torque transducer. Whilst the force was measured by using a load cell (model LCM300-FSH03888). The rotational angle was adjusted by utilizing an Anaheim Automation geared stepper motor with a mechanical brake. The translational motion was created by using an Exlar (model GSX30-1802-MMF-EM2-218) and it

Authorized licensed use limited to: PORTLAND STATE UNIVERSITY LIBRARY. Downloaded on June 09,2024 at 03:02:12 UTC from IEEE Xplore. Restrictions apply.

was driven by utilizing a variable frequency Delta drive (model VFD022C23A).

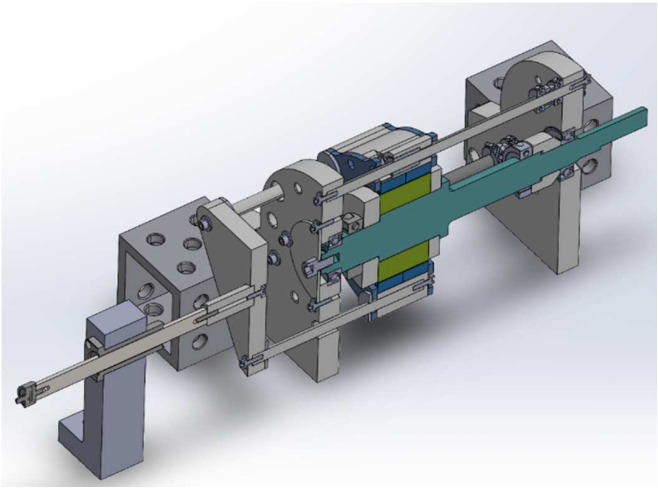

Fig. 8. Assembly drawing

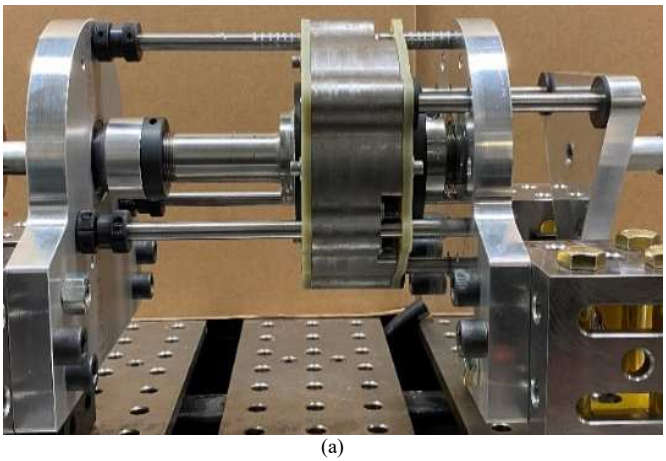

(a)

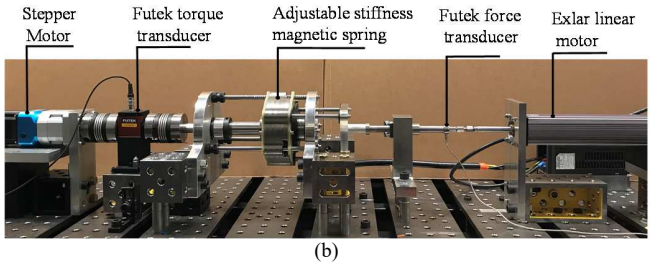

(b)

Fig. 9 (a) Fully assembled single air-gap magnetic spring and (b) test setup.

The experimental measured force and torque results are shown in Fig. 10 and Fig. 11 respectively. A performance summary is shown in Table II a relatively good agreement was obtained. A peak force of 2.6 kN was measured with an energy density of 7.1 J/kg.

TABLE III
ADJUSTABLE STIFFNESS MAGNETIC SPRING PERFORMANCE SUMMARY

Specification	FEA value	Measured value	% Difference	Unit
Peak force	3.0	2.6	-13	kN
Peak torque	73.3	68.1	-7	Nm
Peak stiffness, k_m	100	86	-13	kN/m
Stroke length	30	30	0	mm
Energy density	8.2	7.1	-13	J/kg
Energy	45	39	-13	J

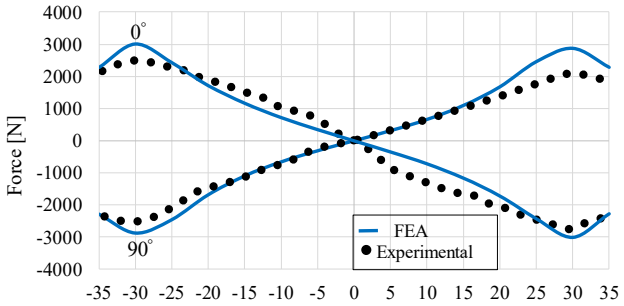

(a)

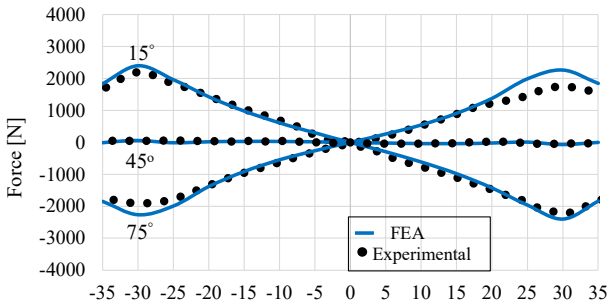

(b)

Fig. 10. Force as a function of stroke length comparison between experimental measurement and finite element analysis value when (a) at the maximum positive and negative stiffness adjusted value (0° and 90°) and (b) at $\theta = 15°$, $45°$ and $\theta = 75°$.

CONCLUSION

This paper presented a new type of variable stiffness magnetic spring. The magnetic spring was shown to exhibits a highly linear stroke length with an adjustable spring constant. Both positive and negative spring stiffness values were shown to be created with equal magnitude and the stroke length exhibits a high degree of linearity. An experimental setup with a peak force capability of 2.6 kN and 30 mm stroke length was utilized to demonstrate and validate

Authorized licensed use limited to: PORTLAND STATE UNIVERSITY LIBRARY. Downloaded on June 09,2024 at 03:02:12 UTC from IEEE Xplore. Restrictions apply.

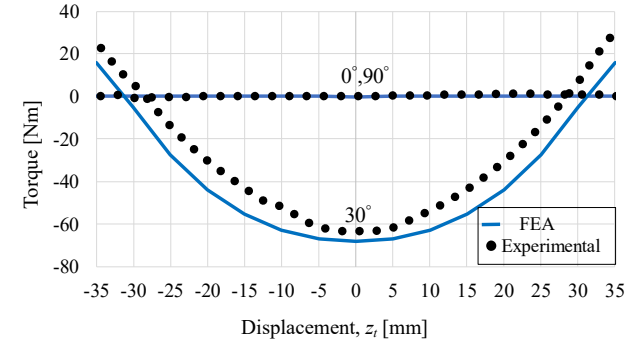

(a)

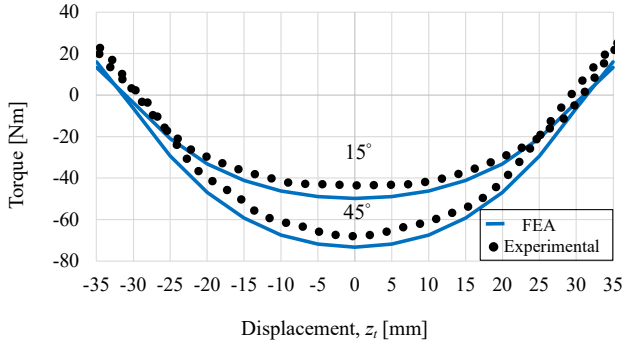

(b)

Fig. 11. Torque as a function of stroke length comparison between experimental measurement and finite element analysis value when (a) at the maximum positive and negative stiffness adjusted value (0° and 90°) and (b) at $\theta = 15°$ and $\theta = 45°$.

the predicted finite element analysis design results.

ACKNOWLEDGEMENTS

The authors would gratefully like to thank the JMAG and Solidworks corporation for the use of their FEA software. The authors would also like to thank Jason Hilbourne and Alexander Ursin, from Utensile, Inc. for their mechanical design assistance.

REFERENCES

[1] D. Rodriguez-Cianca *et al.*, "A variable stiffness actuator module with favorable mass distribution for a bio-inspired biped robot," *Frontiers in Neurorobotics,* vol. 13, no. 20, pp. 1-12, 2019.

[2] G. Tonietti, R. Schiavi, and A. Bicchi, "Design and control of a variable stiffness actuator for safe and fast physical human/robot interaction," in *IEEE Intern. Conf. Robotics Auto.* , Barcelona, Spain, 2005, pp. 526-531.

[3] M. Zhang, L. Fang, F. Sun, X. Sun, Y. Gao, and K. Oka, "Realization of Flexible Motion of Robot Joint with A Novel Permanent Magnetic Spring," in *2018 IEEE International Conference on Intelligence and Safety for Robotics (ISR)*, 24-27 Aug. 2018 2018, pp. 331-336, doi: 10.1109/IISR.2018.8535895.

[4] B. Vanderborght *et al.*, "Variable impedence actuators: a review," *Robotics and Auto. Syst.,* vol. 61, pp. 1601-1614, 2013.

[5] S. Wolf *et al.*, "Variable Stiffness Actuators: Review on Design and Components," *IEEE/ASME Transactions on Mechatronics,* vol. 21, no. 5, pp. 2418-2430, 2016, doi: 10.1109/TMECH.2015.2501019.

[6] A. Sutrisno and D. J. Braun, "How to run 50% faster without external energy," *Science Advances,* vol. 6, no. 13, p. eaay1950, 2020, doi: 10.1126/sciadv.aay1950.

[7] I. N. Ayala-Garcia, P. D. Mitcheson, E. M. Yeatmanb, D. Zhua, J. Tudora, and S. P. Beeby, "Magnetic tuning of a kinetic energy harvester using variable reluctance," *Sensors and Actuators A: Physical,* vol. 189, pp. 266-275, 2013.

[8] T. D. Dang, M. N. Nguyen, and K. K. Ahn, "A Study on Wave Energy Converter with Variable Stiffness Mechanism," in *2019 23rd International Conference on Mechatronics Technology (ICMT)*, 23-26 Oct. 2019 2019, pp. 1-5, doi: 10.1109/ICMECT.2019.8932134.

[9] J. L. G. Janssen, J. J. H. Paulides, E. A. Lomonova, and A. J. A. Vandenput, "Analysis of a variable reluctance permanent magnet actuator," pp. 502-509, 2007.

[10] J. Zhao *et al.*, "Shock Isolation Capability of an Electromagnetic Variable Stiffness Isolator with Bidirectional Stiffness Regulation," *IEEE/ASME Transactions on Mechatronics,* pp. 1-1, 2020, doi: 10.1109/TMECH.2020.3029579.

[11] V. B, V. H. R, L. D, S. T. G, and H. K. W, "Comparison of Mechanical Design and Energy Consumption of Adaptable, Passive-compliant Actuators," *The International Journal of Robotics Research,* vol. 28, no. 1, pp. 90-103, 2009.

[12] G. Mathijssen, P. Cherelle, D. Lefeber, and B. Vanderborght, "Concept of a Series-Parallel Elastic Actuator for a Powered Transtibial Prosthesis," *Actuators,* vol. 2, no. 3, pp. 59-73, 2013. [Online]. Available: https://www.mdpi.com/2076-0825/2/3/59.

[13] H. Li, Y. Li, and J. Li, "Negative stiffness devices for vibration isolation applications: A review," *Advances in Structural Engineering,* vol. 23, no. 8, pp. 1739-1755, 2020, doi: 10.1177/1369433219900311.

[14] A. H. Memar and E. T. Esfahani, "A Robot Gripper With Variable Stiffness Actuation for Enhancing Collision Safety," *IEEE Transactions on Industrial Electronics,* vol. 67, no. 8, pp. 6607-6616, 2020, doi: 10.1109/TIE.2019.2938475.

[15] M. E. Hossain and J. Z. Bird, "Investigating the Performance of a Variable Stiffness Magnetic Spring for Resonant Ocean Power Generation," in *2019 IEEE Energy Conversion Congress and Exposition (ECCE)*, 29 Sept.-3 Oct. 2019 2019, pp. 5002-5008, doi: 10.1109/ECCE.2019.8912306.

[16] W. Wu, X. Chen, and Y. Shan, "Analysis and experiment of a vibration isolator using a novel magnetic spring with negative stiffness," *Journal Sound Vibration,* vol. 333, pp. 2958-2970, 2014.

[17] Y. Bu, K. Inoue, and T. Mizuno, "Dynamically variable negative stiffness structures," *Journal Japan Society Appl. Electro. Mech.,* vol. 23, no. 3, 2015.

[18] Y. Sun *et al.*, "Modeling electromagnetic force and axial-stiffness for an electromagnetic negative-stiffness spring toward vibration isolation," *IEEE Trans. Magn.,* vol. 55, no. 3, p. Art no. 8000410., 2019.

[19] J. O. Rawlings, S. G. Pantula, and D. A. Dickey, *Applied Regression Analysis: A Research Tool*, Second ed. Springer, 1998.

Authorized licensed use limited to: PORTLAND STATE UNIVERSITY LIBRARY. Downloaded on June 09,2024 at 03:02:12 UTC from IEEE Xplore. Restrictions apply.